ISSN 1063-7729, Astronomy Reports, 2007, Vol. 51, No. 1, pp. 19–26. © Pleiades Publishing, Ltd., 2007.
Original Russian Text © O. Ramírez Hernández, E.E. Lekht, A.M. Tolmachev, 2007, published in Astronomicheskiĭ Zhurnal, 2007, Vol. 84, No. 1, pp. 22–29.

Evolution of Selected Components of the H_2O Maser in Sgr B2

O. Ramírez Hernández[1], E. E. Lekht[1,2], and A. M. Tolmachev[3]

[1] *Sternberg Astronomical Institute, Universitetskiĭ pr. 13, Moscow, 119992 Russia*

[2] *Instituto National de Astrophisica, Optica y Electronica, Apartado Postal 51 y 216, Tonanzintla, Puebla, Mèxico*

[3] *Pushchino Radio Astronomy Observatory, Pushchino, Moscow oblast, 142290 Russia*

Received December 12, 2005; in final form, July 7, 2006

Abstract—We present the results of a variability study of some H_2O maser-emission components of Sgr B2, which is located in an active star-forming region. Our monitoring was conducted in 1982–2004 with the 22-m radio telescope of the Pushchino Radio Astronomy Observatory. We analyze brightness variations for the strongest groups of emission features in the H_2O spectra, mainly during periods of maser flaring activity. Each of these groups contains many components, whose radial velocities and fluxes we determined. Most of the components displayed radial-velocity drifts. We detected a correlation between the flux and radial-velocity variations for some of the components. Variability of the emission can be explained in a model in which the maser spots form elongated chains and filaments with radial-velocity gradients. During H_2O flares, the flux increases of some maser spots were accompanied by acceleration, while flux decreases were accompanied by deceleration of their motion in the dense circumstellar matter. Spectral groups of emission features are probably spatially compact structures.

PACS numbers : 98.38.Er, 95.85.Bh, 98.35.Ac, 98.38.Dq
DOI: 10.1134/S1063772907010027

1. INTRODUCTION

Sgr B2 is one of the most complex and active star-forming regions in our Galaxy. It contains many individual HII regions with quite different morphologies [1–3]. Three main sites of star formation have been identified: Sgr B2 N, Sgr B2 M, and Sgr B2 S [4]. According to Kobayashi et al. [5] and McGrath et al. [6], H_2O maser emission is observed from each of these three sites. The N and M regions are the largest, and the N region is believed to be younger [2].

The strong H_2O emission from Sgr B2 M is mainly related to a compact group of maser spots projected onto the super-compact HII region F1 [5], as well as a bipolar molecular flow. According to VLA observations [6] made on June 6, 1998, the H_2O masers are predominantly located in the region of the 7-mm continuum [7] with high gas velocities. Stellar wind can also play an important role in exciting the maser H_2O emission. The radial velocity determined using the integrated emission in the H76α hydrogen recombination radio line for Sgr B2 M is 61.5 km/s [8]. The H_2O emission was strongest at 60–70 km/s, near the velocity of the HII region.

Sgr B2 N is associated with a rotating accretion disk of molecular gas, with three embedded super-compact HII regions [9]. The strongest maser activity is related to the region K2 and the dynamical center of the molecular flow [10], which may be the source of excitation for the maser emission. For this source, the integrated emission in the H76α line gives $V_{\rm LSR} \approx$ 70 km/s [8].

Lekht et al. [11] demonstrated that Sgr B2 N and M alternate as dominant sources of the integrated H_2O emission, with Sgr B2 M becoming dominant after late 2003.

The complex structure of Sgr B2 and the presence of many individual maser spots and spot groups result in a very complex shape for the total H_2O line profile. When observing with single antennas, the most favorable periods for studies of the structure and evolution of individual components are periods of the maser flare activity. The present paper is devoted to studies of this kind.

2. OBSERVATIONS

Our monitoring was performed in the direction of Sgr B2 in the H_2O line at $\lambda = 1.35$ cm using the 22-m radio telescope of the Pushchino Radio Astronomy Observatory in 1982–2004 [11–13]. The mean time interval between the observations was about 1.5 months. After the modernization of the equipment complex in 2000, the system noise temperature was

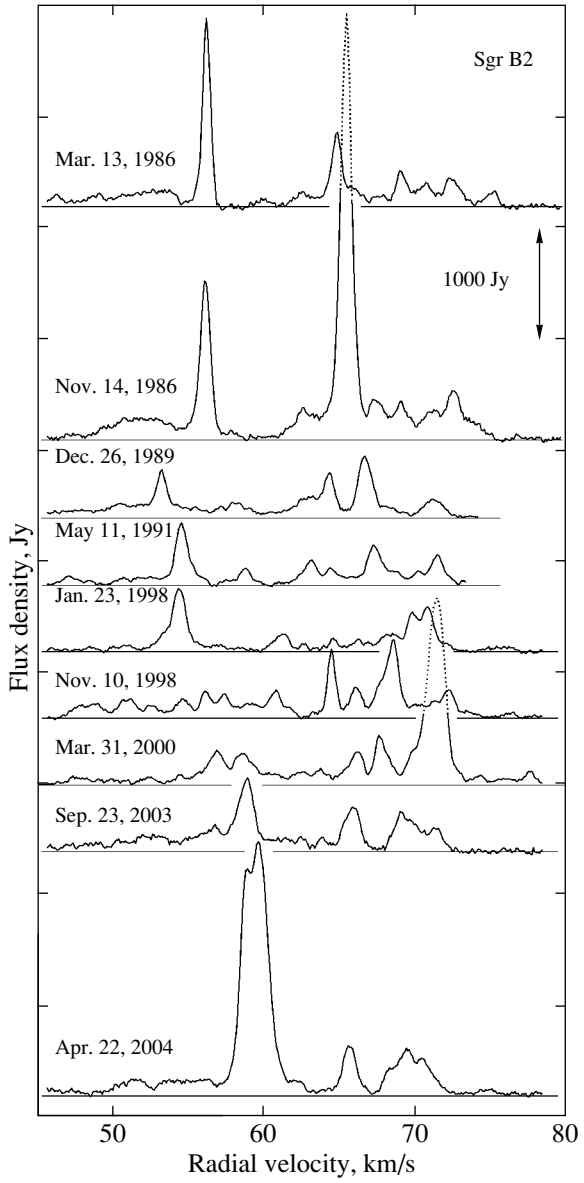

Fig. 1. Selected H_2O maser-emission spectra for Sgr B2 observed during epochs of strong flares. The double arrow indicates the scale along the vertical axis.

100–150 K. The signal analysis was performed using a 128-channel filter-type spectral analyzer with a spectral resolution of 7.5 kHz (0.101 km/s in radial velocity). The antenna beam width at 22 GHz is 2.6′.

We corrected the H_2O spectra for the absorption in the Earth's atmosphere. Figure 1 displays the most typical H_2O maser spectra acquired at various epochs when strong flares of the emission occurred [11–13]. We selected several parts of the spectrum for our analysis. Since we are concerned here with an analysis of individual maser spots or clusters of spots, our main selection criterion was the presence of strong flares in one or several emission features, regardless of their relation to a particular source (Sgr B2 M or N).

Since all of the spectral fragments selected for our analysis are complex, and contain many components with similar radial velocities, we fitted Gaussians to the line profiles. To get better insight into the number of line components and their positions in the spectra, we also analyzed the line profile shapes and their variations in time. The results of decomposing the lines into individual components are presented in Figs. 2–5, in chronological order. We did not analyze the spectra for 1993.5–1997.5 due to the low activity of the maser and the large time gaps between consecutive observations.

Figure 2 shows the results of our detailed analysis for the two main components (56 and 66 km/s) of a superflare of Sgr B2 N in 1985–1987 [11]. The upper panel presents the decomposition of the 56 km/s component into three individual features (marked *1a, 1b, 1c*). The middle panel is the same for the 66 km/s component, with the positions of the main emission features (*2a, 2b, 2c, 2d, 2e, 2f*) and other emission features in their immediate vicinity indicated. The solid circles identify the main features of the flare at 66 km/s, as well as features with fluxes in excess of 400 Jy before and after the strong flare.

The bottom panel presents the flux variations for the main components (*1a, 1b, 1c* and *2a, 2b, 2c, 2d, 2e, 2f*). Since the main features exhibit high flux levels, it was not always possible to determine the fluxes of neighboring features in the ascending and descending branches of their evolution. We connected the flux variability curves for the main features (dashed curves for feature *2*). As a result, the curves obtained for the flares at 56 and 66 km/s reflect variations of the emission maxima.

Figure 4 also presents VLA results for epoch 1998.44 taken from McGrath et al. [6] (the symbols are the same as in Fig. 2). The large circles with central crosses refer to Sgr B2 N and the large solid circles to Sgr B2 M. The corresponding fluxes are given near these symbols. The components at 68.7 and 74 km/s consist of several emission features, and the combined fluxes of these features [6] are shown for these velocities. It appears that our decomposition of the spectra into individual components is sufficiently correct and complete. Note that the VLA observations had a spectral resolution of 0.66 km/s, compared to the resolution of 0.1 km/s for our monitoring. This enabled us to follow the evolution of components with rather fine structure.

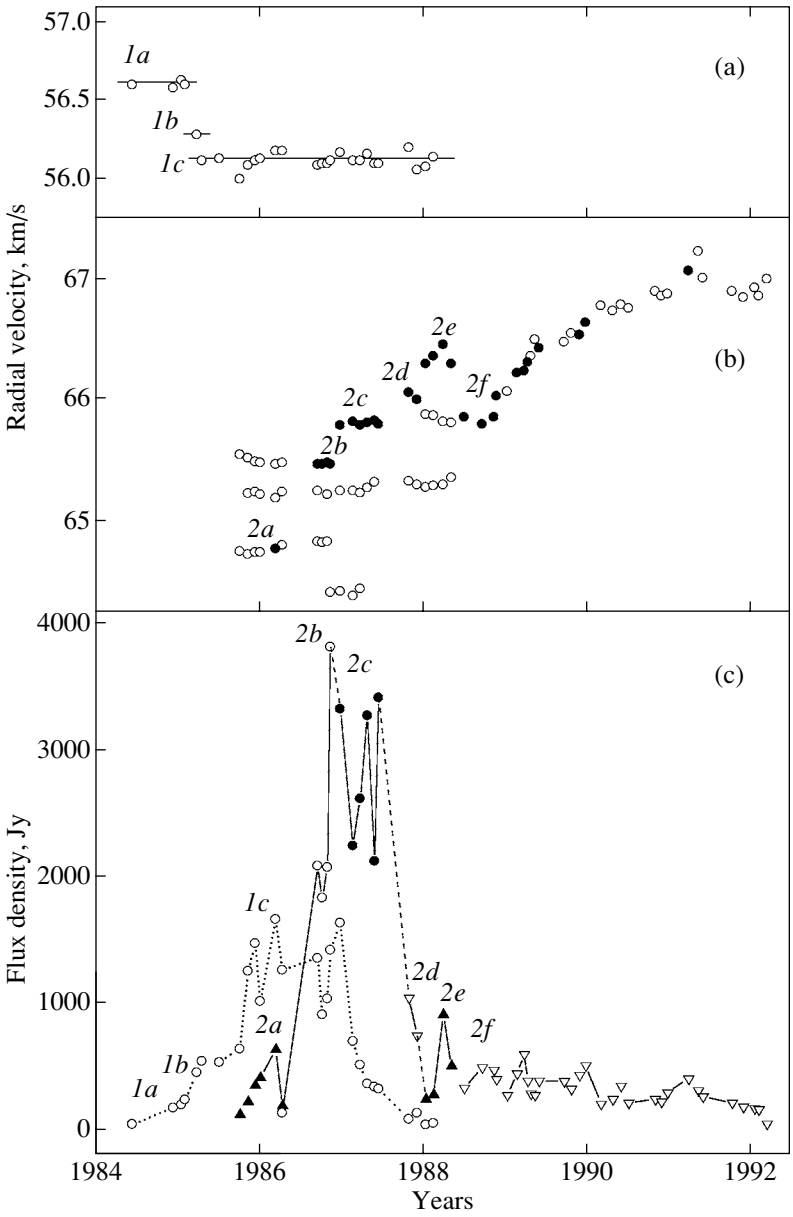

Fig. 2. Variations of radial velocities and fluxes for individual components of the H_2O spectrum in the velocity intervals 55.5–57 and 64.5–67.5 km/s in 1984–1992 (the symbols are explained in the text).

3. DATA ANALYSIS

Figure 1 shows that high activity of the H_2O masers in the Sgr B2 complex was observed virtually in the entire radial-velocity range, 52–73 km/s. Two strong flares were observed in 1986–1987 and 2004. The first of these was associated with Sgr B2 N [11] and the second with Sgr B2 M [13]. Their energies were almost comparable to the superflare in Orion in 1979–1987.

3.1. H_2O Maser Flares

The emission of most of the H_2O spectral components was flaring, with the highest fluxes being 300–1000 Jy. Stronger flares in individual features were observed from time to time, with fluxes as high as 3000–4000 Jy. The flare durations were from a month to 1.5 years. The line widths for individual components were quite large (0.7–1 km/s), sometimes reaching 2 km/s, unlike those observed for other sources associated with star-forming regions. As a rule, strong flares were comprised of sequences of flares in individual features (Figs. 2 and 3; the symbols used for the components and feature in Fig. 3 are the same as in Fig. 2).

Flaring features can have either similar or very different radial velocities. For example, the strongest

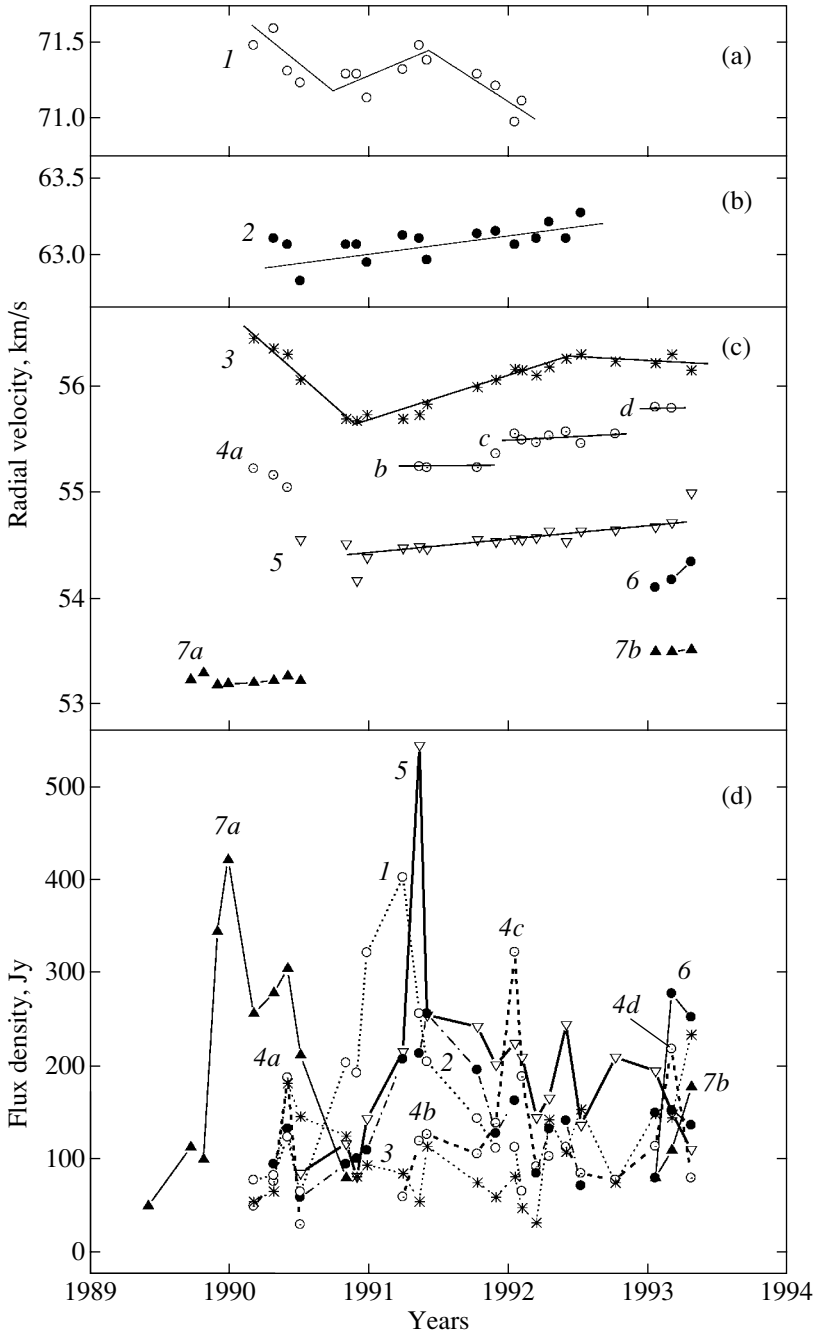

Fig. 3. Same as in Fig. 2 for the 53–57, 62.5–63.5, and 70.8–71.8 km/s in 1989–1993.

emission during the 1985–1987 flare in Sgr B2 N appeared first at $V_{\rm LSR} \approx 56.1$ km/s with a peak flux of 1650 Jy, then at $V_{\rm LSR} \approx 66$ km/s with a flux as high as 3800 Jy [11] (Fig. 2). The strongest emission during the flare at 56 km/s was that from the feature at the "blue" side (feature *1c*). The flux in this feature exceeded 1000 Jy for 1.5 years, while its radial velocity was constant during these 1.5 years, as well as during the entire next year.

The evolution of the flare at 66 km/s was much more complex. We detected the beginning of the flare in September 1986. The line profile was asymmetric. The line width at the half-maximum level was about 1 km/s. The line consisted of two main components (Fig. 2), the main one at $V_{\rm LSR} \approx 65.5$ km/s. By the end of 1986, the line width decreased to 0.8 km/s, and the main component split. A similar event occurred in early 1988, and abrupt velocity changes were observed in late 1988 and early 1989. The observed

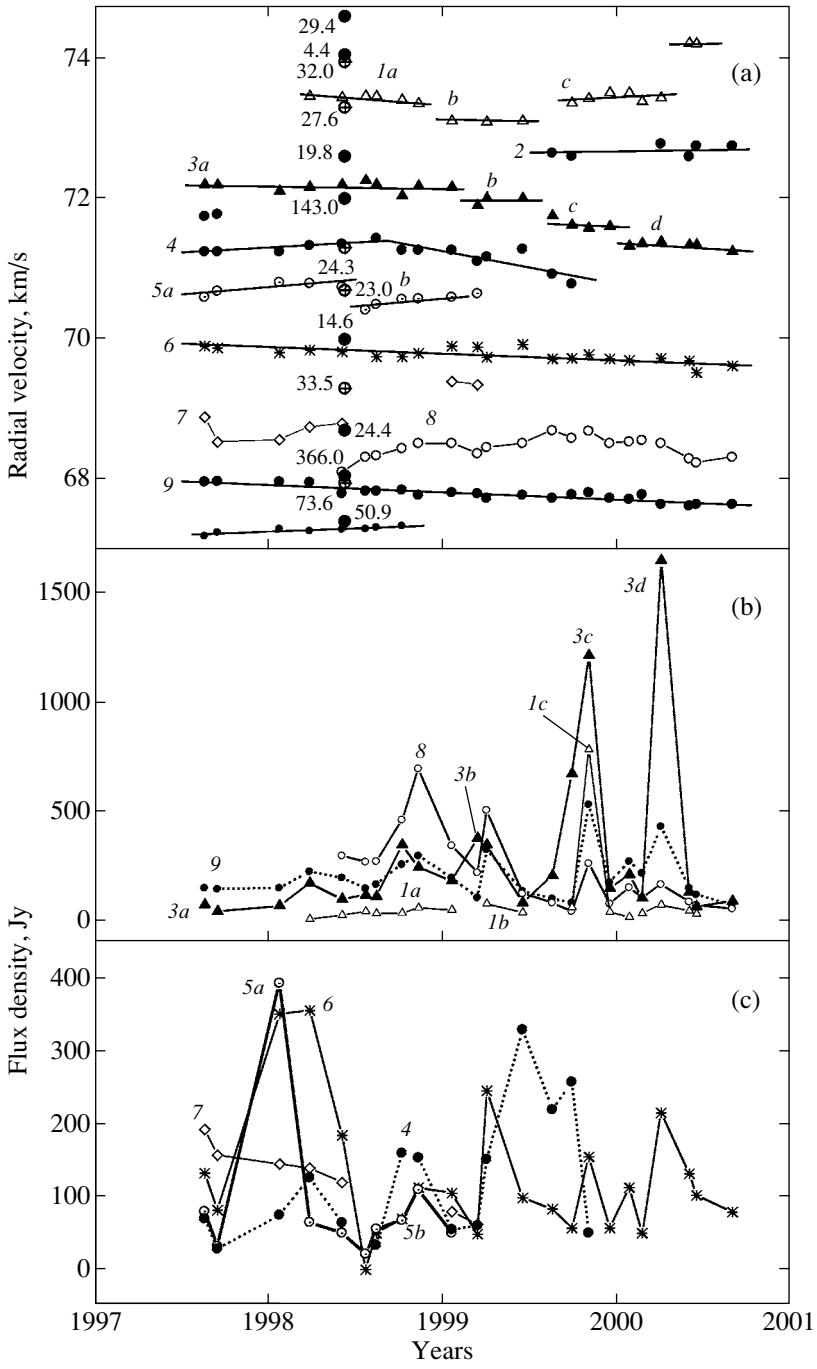

Fig. 4. Results of the decomposition of the H_2O spectrum into individual components at 67.5–74.5 km/s (1997–2000). The large circles with central crosses and large solid circles are the positions of the northern and main sources, respectively for epoch 1998.44 [6]. (Other symbols are explained in the text.)

pattern for the evolution was restricted to the velocity range 64–67 km/s.

It both flares, the lines were broad and, because of their complex structure, asymmetric at the early stages. Their evolution consisted of the consecutive appearance and decay of emission features in order of increasing or decreasing radial velocity, indicating fragmentation of the medium and the presence of gradients of V_{LSR}. The most complex region is responsible for the flare at 66 km/s. It probably contains fairly persistent clumps of matter (maser spots) with

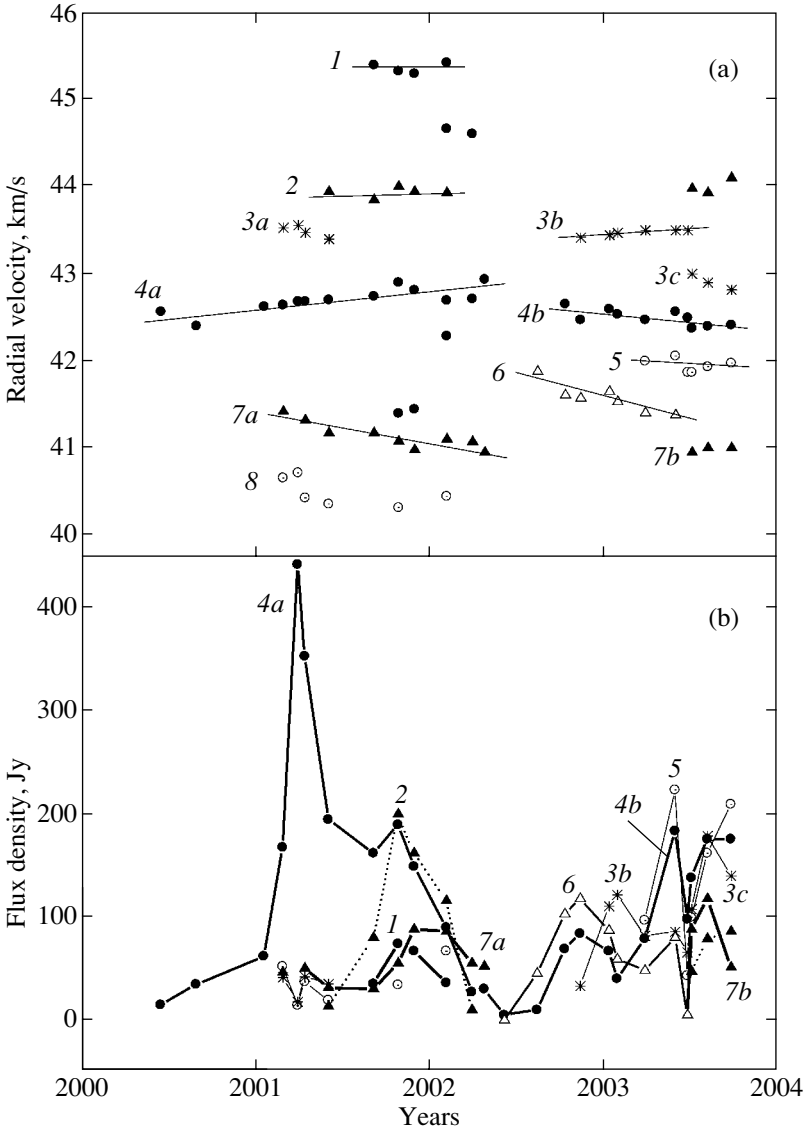

Fig. 5. Same as in Fig. 4 for 40–46 km/s.

similar radial velocities. We isolated at least six such structures.

According to Lekht et al. [11], the two regions responsible for the superflare are located in the molecular outflow of Sgr B2 N. The velocity gradients can have opposite signs if the regions are situated in different parts of the molecular flow. This is also required by the fact that the radial-velocity difference of these components, 10 km/s, is fairly large. The time lag between the flares at 56 and 66 km/s was eight to nine months. Since the stellar-wind velocity is roughly 500 km/s, the corresponding distance between the regions responsible for the flares is $\sim 1.1 \times 10^{15}$ cm.

3.2. Radial-Velocity Drift

In addition to strong flux variations, most of the emission features exhibited a radial-velocity drift. The drift has a large variety of modes. A typical case was a more or less smooth radial-velocity variation, for example, for features *2f* (Fig. 2), *2* and *5* (Fig. 3), as well as features *6* and *9* at 68 and 70 km/s (Fig. 4). In this case, the rate of the velocity variation was not large, only occasionally reaching 0.4–0.5 km/s per year.

In some other cases, the radial velocities changed abruptly by 0.1–0.3 km/s. Such components were often found to contain several links. For example, feature *1* (Fig. 2) has three links and feature *4* at 55.5 km/s (Fig. 3) has four links and a radial-velocity

gradient. The same is true for feature *3* at 72 km/s (Fig. 4); each element of this chain had its own flux peak.

We also observed the coexistence of the two drift types, as well as more complex radial-velocity variations. Component *1* in Fig. 3 (71.2 km/s) demonstrated correlated flux and radial-velocity variations (Fig. 3). The velocity increased with flux; i.e., the motion of the maser condensation was accelerating. During the flux decline, V_{LSR} decreased. Apparently, the condensation was decelerated in the dense circumstellar medium during the descending branch of the flare's evolution.

The approximation of the V_{LSR} drift for feature *3* in Fig. 3b is not the only one possible. The velocity drift in one direction could be due to acceleration of the maser spot's motion by the stellar wind. When the stellar wind became less strong, the velocity drift changed direction due to deceleration of the spot in the dense circumstellar medium. However, this spot showed no correlation between its flux and velocity variations, unlike the component at 71.2 km/s. For this reason, we suggest that maser spot *3* is a non-uniform filament, with different velocities along it.

3.3. Model of the H_2O Components

The variety of variability types for individual emission features and for groups of features with similar radial velocities leads to several possible models. Note again the large line widths, reaching 1–1.5 km/s. Individual lines that broad are not characteristic of most water masers associated with star-forming regions. Possible origins of the broadening were considered in [11], where it was assumed that the maser spots were elongated and that turbulent motions occurred within them. This leads to broadening and, in certain cases, asymmetry of the components.

The observed velocity jumps suggest that the elongated spots are subdivided into individual clumps of matter, resembling individual links in a kind of chain. A shock due to the interaction between the stellar wind and dense medium passes these links one after another, exciting their maser emission. In this case, we observe a correlation between maser-emission peaks and the corresponding elements of the chain (like for emission at 72 km/s in Fig. 4).

The maser spots demonstrating a smooth velocity drift, without jumps, can be elongated (like filaments) but without fragmentation into individual clumps. The components with more complex radial-velocity drifts (like the component at 71.2 km/s in Fig. 3) appear to represent another type of maser spot. Their correlated flux and radial-velocity variations can also be explained in a model where a matter clump is accelerated by the stellar wind, then decelerated in the circumstellar medium when the wind becomes less strong.

The regions related to the flares of 1985–1987 have a complex structure and consist of many maser spots. In these regions, individual maser spots are probably fairly stable.

The absence of a significant time lag between the flux maxima of emission features with similar V_{LSR} values suggests that we are dealing with close and compact groups of features.

4. RESULTS

High flare-like activity of the H_2O maser in the Sgr B2 complex was observed fairly frequently during our 24-year monitoring. Thus, we were able to follow the evolution of individual components. Our high spectral resolution and the fact that our observations were fairly frequent enabled us to study the structures of individual maser spots during their enhanced activity. The main results of our study are listed below.

(1) We detected radial-velocity drifts for most of the H_2O spectral components (maser spots).

(2) The flux and radial-velocity variations observed for a line's individual spectral features can be explained in a model in which the maser spots form elongated chains or filaments, with a radial velocity gradient along this structure.

(3) The stellar wind has a strong influence on individual maser spots, e.g., accelerating them. When the stellar wind becomes less strong, the spot is apparently decelerated in the circumstellar medium, reversing the direction of the velocity drift.

(4) The large observed line widths of individual maser components (0.8–1.5 km/s) may indicate that they are non-uniform, and contain considerable turbulence.

(5) The spectral groups of H_2O emission features with similar radial velocities probably form compact spatial structures.

REFERENCES

1. R. A. Gaume, M. J. Claussen, C. G. De Pree, et al., Astrophys. J. **449**, 663 (1995).
2. C. G. De Pree, R. A. Gaume, W. M. Goss, et al., Astrophys. J. **451**, 284 (1995).
3. C. G. De Pree, W. M. Goss, and R. A. Gaume, Astrophys. J. **500**, 847 (1998).
4. J. M. Benson and K. J. Johnston, Astrophys. J. **277**, 181 (1984).
5. H. Kobayashi, M. Ishiguro, Y. Chikada, et al., Publ. Astron. Soc. Jpn. **41**, 141 (1989).

6. E. J. McGrath, W. M. Goss, and C. G. De Pree, Astrophys. J., Suppl. Ser. **155**, 577 (2004).
7. S. Y. Lui, D. M. Mehringer, Y. Miao, and E. Snyder, Astrophys. J. **501**, 680 (1998).
8. P. R. Roelfsema, W. M. Goss, J. B. Whiteoak, et al., Astron. Astrophys. **175**, 219 (1987).
9. R. A. Gaume, W. M. Goss, and M. J. Claussen, Astrophys. J. **464**, 788 (1996).
10. D. C. Lis, P. F. Goldsmith, J. E. Carlstrom, et al., Astrophys. J. **402**, 238 (1993).
11. E. E. Lekht, O. Ramírez Hernández, and A. M. Tolmachev, Astron. Zh. **81**, 1059 (2004) [Astron. Rep. **48**, 965 (2004)].
12. E. E. Lekht, O. Ramírez Hernández, A. M. Tolmachev, and I. I. Berulis, Astron. Zh. **81**, 195 (2004) [Astron. Rep. **48**, 171 (2004)].
13. O. Ramírez Hernández, E. E. Lekht, and A. M. Tolmachev, Astron. Zh. **82**, 874 (2005) [Astron Rep. **49**, 777 (2005)].

Translated by N. Samus'